Title

Transformable amyloid-beta mimetic peptide amphiphiles for lysosomal disruption in non-small cell lung cancer

Authors

Baehr, Christopher M
Zhang, Lu
Wu, Yi
et al.

Publication Date

2021-10-01

DOI

10.1016/j.biomaterials.2021.121078

Peer reviewed

HHS Public Access

Author manuscript

Biomaterials. Author manuscript; available in PMC 2023 February 27.

Published in final edited form as:

Biomaterials. 2021 October ; 277: 121078. doi:10.1016/j.biomaterials.2021.121078.

Transformable Amyloid-Beta Mimetic Peptide Amphiphiles for Lysosomal Disruption in Non-Small Cell Lung Cancer

Christopher M. Baehr[1], **Lu Zhang**[1], **Yi Wu**[1,2], **Andras Domokos**[1,4], **Wenwu Xiao**[1], **Lei Wang**[1,3], **Kit S. Lam**[1]

[1]Department of Biochemistry & Molecular Medicine, University of California Davis, School of Medicine, 2700 Stockton Blvd, Sacramento, California 95817, USA

[2]Institute of Traditional Chinese Veterinary Medicine, College of Veterinary Medicine, Nanjing Agricultural University, #1 Weigang, Nanjing 210095, Jiangsu Province, PR China

[3]CAS Center for Excellence in Nanoscience, CAS Key Laboratory for Biomedical Effects of Nanomaterials and Nanosafety, National Center for Nanoscience and Technology, Beijing 100190, China.

[4]Department of Chemistry, University of California, Davis, One Shields Ave, Davis, California, 95616, USA.

Abstract

Non-small cell lung cancer (NSCLC) is the largest contributor to cancer mortality in the United States. Traditional chemotherapies are toxic and prone to the development of drug-resistance. Recently, several drug candidates were shown to induce lysosomal membrane permeabilization (LMP) in aggressive cancers. This has led to increased interest in lysosome dysregulation as a therapeutic target. However, approaches are needed to overcome two limitations of current lysosomal inhibitors: low specificity and potency. Here, we report the development of a transformable nanomaterial which is triggered to induce LMP of lysosomes in NSCLC. The nanomaterial consists of peptide amphiphiles, which self-assemble into nanoparticles, colocalize with the lysosome, and change conformation to nanofibrils due to lysosomal pH shift, which leads to the disruption of the lysosome, cell death, and cisplatin sensitization. We have found that this cell-penetrating transformable peptide nanoparticle (CPTNP) was cytotoxic to NSCLC cells in the low-micromolar range and it synergized cisplatin cytotoxicity four-fold. Moreover, we

kslam@ucdavis.edu .

Declaration of interests

The authors declare that they have no known competing financial interests or personal relationships that could have appeared to influence the work reported in this paper.

CRediT Author Statement

CB conceived the original concept with help from LW. CB fabricated samples with the help of LZ. CB developed the experimental plan with guidance from LZ, LW, and KL. AD helped with the chemical characterization of the peptides, while YW and WX helped with in vivo experiments. The manuscript was written primarily by CB, all authors contributed significant feedback and additions. All authors have given approval to the final version of the manuscript.

demonstrate CPTNP's promising antitumor effect in mouse xenograft models with limited toxicity when given in combination with low dose cisplatin chemotherapy. This is the first example of enhanced LMP via transformable peptide nanomaterial and offers a promising new strategy for cancer therapy.

Keywords

Nanoparticles; Nanofibers; Non-Small Cell Lung Cancer; Cisplatin; Amyloid-Beta; Lysosomal targeting

1. Introduction

Lung cancer accounts for the plurality of cancer instances and deaths both in the US and abroad.[1] Despite the advent of immune checkpoint blockade and other targeted therapies, platinum-based chemotherapy is still the most common therapeutic regimen for patients with stage II to stage IV non-small cell lung cancer (NSCLC).[2] Unfortunately high dose cisplatin therapy is poorly tolerated and only moderately improves the 5-year survival rate of patients.[3] As such, there is a necessity for novel therapeutics which synergize with traditional cytotoxic chemotherapies; thus, allowing for the use of lower chemotherapeutic doses and a reduction in adverse side effects.

Since the lysosome's discovery in 1955 by Christian de Duve, it has traditionally been conceptualized as the proteolytic 'garbage bag' of the cell.[4] However, current research demonstrates that the lysosome is central to various cellular processes including nutrient scavenging, tissue remodeling and metabolic regulation.[5] Interestingly, lysosomal aberrations such as changes in lysosomal volume, autophagic dysregulation,[5] and cellular distribution of lysosome associated proteins have been observed in many cancer lines.[4] These lysosomal alterations correlate well with angiogenesis and cancer metastasis,[1] and are mediated via downregulation in lysosomal-associated membrane protein 1 & 2 (LAMP1,2), up-regulation of oncogenes Src and Ras, and alteration of the localization of HSP70.[2] While changes centered around lysosomal metabolism and exocytosis confer a proliferative advantage to cancer cells,[3–6] they also promote instability of the lysosomal membrane, making lysosomal membrane permeation (LMP) a promising cancer therapeutic target.[7] Several lysosomal inhibitors have been reported to selectively induce LMP in cancer cells explicitly.[8] Salinomycin selectively targets cancer stem cells by inducing lysosomal sequestration of iron and inducing ferroptosis.[9] Other agents such as oleocanthal, a compound found in olive oil, selectively induce cancer cell death by inhibiting acid sphingomyelinase, thereby selectively inducing LMP.[10] Chloroquine, an anti-malarial drug currently being studied in several human cancer trials for its synergistic effect with common chemotherapies, is traditionally thought of as an autophagy inhibitor, although some evidence suggests that it also induces LMP at high doses.[11,12] Nanomaterials with autophagic inhibitory activity are also being investigated.[13] Despite showing promise, these drugs all suffer from low selectivity for the lysosome and low potency, therefore novel LMP inducing therapeutic agents with improved targeting and potency are needed.

Supramolecular chemistry involves the self-assembly of subunits by non-covalent interactions. Our group and others have explored the development of amyloid beta mimetic peptide amphiphiles.[14–18] The nanoparticles self-assembled from peptide amphiphiles transform into nanofibers with β-sheet structure, which may be triggered by either ligand-receptor interactions,[19–21] pH,[22] or hydrophobic-hydrophilic modulation. Other groups have developed triggerable nanofiber forming peptides which target the cytosol[23] and the mitochondria[18], however, no triggerable peptide nanoparticle has been developed to target the lysosome, despite the lysosome's promise as a cancer therapeutic target.[6,24,25] Here we explore the development of a pH-sensitive transformable peptide nanoparticle, comprised of beta-amyloid mimetic peptide amphiphiles. These cell-penetrating transformable peptide nanoparticles (CPTNPs) are designed to be up-taken by NSCLC cells, localize to the lysosome and transform into high aspect ratio nanofibers (Figure 1) due to acidic pH shift. These nanofibers induce LMP and lysosomal disruption which facilitates cell death. The nanoplatform contains three distinct motifs. First, a hydrophilic, cell penetrating, poly-*D*-Arg motif (8-mer). Poly-arginine is a well-known cationic cell penetrating peptide which has previously been demonstrated to target the lysosome when associated with macromolecules.[26,27] Second, an all *D*-amino acid containing β-sheet forming motif (kffvlk). *D*-amino acids containing peptides are expected to resist proteolytic degradation inside the lysosome. This sequence (in L-amino acids) has previously been explored by us and by others as a nanoparticle-nanofiber forming motif.[21] Third, bis-pyrene (BP) which acts as both a strong hydrophobic group and a dye for tracking of the nanoparticles. The transformation of CPTNPs may be explained by the shift in π-π interaction between phenylalanine side chains, as explored by others.[28] In this study, we demonstrate the capacity of CPTNPS to be taken up by clathrin-mediated endocytosis (CME), lysosomal delivery, and intra-lysosomal transformation of the nanomaterial, resulting in permeation of the lysosomal membrane. In addition, we were able to demonstrate that CPTNP could induce cancer cell death in the low μM range, sensitize cisplatin anti-cancer activity, and reduce tumor burden of xenograft model *in vivo*, with limited toxicity.

4. Methods

Peptide synthesis:

Peptide monomers were synthesized via solid-phase peptide synthesis using standard fluorenylmethyloxycarbonyl (Fmoc) chemistry and Ethyl cyano(hydroxyimino)acetate (Oxyma)/1,3-Diisopropylcarbodiimide (DIC) coupling as described in previous publications.[29] Rink amide MBHA resin (loading 0.503 mmol/g, P3 BioSystems, Louisville, KY) was used as solid support. A 6-fold molar excess of Fmoc-protected amino acids to resin was used for coupling. The reaction was monitored with ninhydrin test. The Fmoc group was de-protected with 20% 4-methylpiperidine in N,N-dimethylformamide (DMF) (first 5 min, then 15 min). After the last cycle of amino acids coupling and Fmoc-deprotection, the linear biotinylated peptide was cleaved with a trifluoroacetic acid (TFA) cocktail containing 90% TFA, 5% thioanisole, and 5% H_2O. The liquid was collected and precipitated in cold (−20°C) diethyl ether and subsequently washed 3 times. The powder was re-dissolved in small amount of 50% ACN/water and analyzed by reversed-phase high performance liquid chromatography (RP-HPLC) on a preparative Vydac C18 column. The purity was

determined to be >95%. The identities of peptides were confirmed Matrix-Assisted Laser Desorption/Ionization-Time of Flight (MALDI-TOF) and ^{1}H Nuclear Magnetic Resonance (NMR) using a 400 MHz Bruker spectrometer, with samples prepared in d_6-DMSO. CPTNP-FF (Figure 2, A): ^{1}H NMR (400 MHz, DMSO-d_6) δ 8.44 – 8.08 (m, 18H), 8.00 (s, 7H), 7.89 (s, 6H), 7.74 (s, 4H), 7.69 (s, 2H), 7.61 (s, 3H), 7.51 (s, 1H), 7.48 – 6.70 (m, 48H), 4.61 (s, 1H), 4.48 (s, 2H), 4.38 – 3.94 (m, 23H), 3.51 (s, 12H), 2.99 (s, 3H), 2.89 (s, 2H), 2.83 – 2.61 (m, 10H), 2.42 – 1.82 (m, 12H), 1.40 – 1.29 (m, 7H), 1.23 (s, 9H), 1.15 (t, J = 6.9 Hz, 2H), 1.10 (d, J = 2.3 Hz, 2H), 0.85 (d, J = 14.2 Hz, 17H); (Figure S2). HRMS (MALDI-TOF) m/z: $[M+H]^+$ Calc'd for $C_{135}H_{191}N_{41}O_{18}H$ 2675.53; Found 2675.649, (Figure S1). CPTNP-GG (Figure 2, B): ^{1}H NMR (400 MHz, DMSO) δ 8.39 (dd, *J* = 14.7, 7.6 Hz, 4H), 8.33 – 8.22 (m, 8H), 8.18 (s, 1H), 8.16 (s, 3H), 8.15 – 8.09 (m, 6H), 8.09 – 7.94 (m, 9H), 7.93 – 7.73 (m, 8H), 7.70 (s, 2H), 7.64 (s, 2H), 7.51 (s, 1H), 7.21 (s, 44H), 4.22 (s, 13H), 4.11 (s, 4H), 3.87 – 3.68 (m, 9H), 3.51 (s, 9H), 2.99 (s, 2H), 2.89 (s, 2H), 2.73 (d, *J* = 17.5 Hz, 5H), 2.16 (p, *J* = 7.3 Hz, 3H), 2.03 – 1.92 (m, 3H), 1.38 (s, 5H), 1.23 (s, 12H), 1.17 – 1.13 (m, 3H), 1.11 (d, *J* = 2.3 Hz, 1H), 0.91 – 0.74 (m, 20H).HRMS (MALDI-TOF) m/z: $[M+H]^+$ Calc'd for $C_{121}H_{179}N_{41}O_{18}H$ 2495.44; Found 2495.960, (Figure S1).

Nano-formulation:

Peptide powder was dissolved in DMSO at concentration 20mM and allowed to sonicate for approximately one hour or until all solids were dissolved and solution was clear, similar to our other publications.[19,21] To form nanoparticles DMSO solubilized monomers were rapidly pipetted into PBS (or a phosphate-citrate) solution buffered at pH 7.4. The solution is then vigorously vortexed for 30 seconds. To form nanofibers, the nanoparticle solution is diluted into an acidic phosphate-citrate buffer solution to achieve a final pH < 5.0.

Characterization of Nanomaterials:

The size distribution of nanoparticles was carried out via dynamic light scattering instrument (DLS, Nano ZS, Malvern) at 25 °C. The concentrations of the nanoparticles were 40μM for DLS measurements. Transmission Electron Microscopy (TEM, Philips CM-120) samples were prepared by dipping a copper grid into 40μM solution of nanomaterials. Grids were allowed to dry at room temperature, and morphology observed. Absorbance and fluorescence spectra were measured on a microplate reader (SpectraMax M3, USA).

In Vitro studies:

All cells were cultured in DMEM (Thermo Fisher: 11960044) with 10% FBS and penicillin/streptomycin, with the exception of HPAepic cells which were cultured similarly with the addition of 1X Insulin-Transferrin-Selenium (Thermo Fisher: 41400045). All cells were procured from American Type Culture Collection (ATCC) with the exception of HPAepic which were procured from ScienCell.

To evaluate the *in vitro* cytotoxicity of CPTNPS, nanomaterial was incubated with various cancer cell lines for 72 h and analyzed by 3-(4,5-dimethylthiazol-2-yl)-5-(3-carboxymethoxyphenyl)-2(4-sulfophenyl)-2H-tetrazolium) (MTS) assay.

All microscopy was carried out on a Zeiss LSM 800 confocal microscope unless otherwise specified. Image quantification was preformed using imageJ. For all studies at least 5 images were quantified per well with at least 40 cells per well. The 5 images were averaged (1 replicate) and at least 3 wells were averaged. Statistics were analyzed via GraphPad Prism 6.0. For FITC dextran assays the protocol from Aits *et al*, January 2015, with little modification was followed.[30] For Galectin Puncta assays the protocol outlined in Aits *et al*, August 2015, was used.[31] In this case the galectin-1 antibody from abcam (ab25138) was used with secondary Goat anti-Rabbit IgG, Alexa Flour 568 procured from Thermo Fisher (A11011). Lysotracker red (Ex/Em:577/590nm) and green (Ex/Em:504/511nm) was procured from Thermo Fisher (Catalog number: L7528 and L7526 respectively). Texas Red labeled cisplatin (TR-Cisplatin, Ex/Em: 568/603nm) was procured from Ursa Biosciences. For the detection of Cisplatin DNA adducts a rat Anti-cisplatin monoclonal antibody was procured from Sigma-Aldrich (MABE416). Anti-clathrin. For Annexin V/PI flow cytometry the Dead Cell Apoptosis Kit from thermofisher (V13241) was used. Flow cytometry was performed on a desktop Guava easyCyte. For Caspase 3 western blot the anti-caspase 3 antibody from abcam was used (ab4051).

In Vivo studies:

Nude mice, 4~5 weeks of age, were ordered from the Jackson laboratory (Sacramento, CA). All animal procedures were performed under the requirements of institutional guidelines and according to protocol No.19724 approved by the Use and Care of Animals Committee at University of California, Davis. A549 cells in PBS and Matrigel suspension (1:1 vol/vol) were injected subcutaneously into the right flank of nude mice. The tumor sizes for all nude mice were monitored and recorded at least bi-weekly. Tumors reaching the dimensions of >100 mm^3 were used for biodistribution and treatment study.

Athymic mice bearing A549 NSCLC xenografts were used for the *in vivo* therapeutic studies (n=6/group). Nanomaterials and PBS were injected via tail vein, eight doses, every third day along with IP cisplatin as reported. Tumor volume and body weight were measured several times per week. Once the humane endpoint was reached, tumor volume greater than 2000 mm^3 the mice were sacrificed, and blood was harvested for evaluation.

Statistical analysis:

All data was analyzed using Graphpad Prism 6.0 software. All results were presented as mean ± standard deviation unless otherwise noted. Comparisons between two groups were analyzed with an unpaired students T test. In the case of multiple comparisons, the Analysis of Variance test was used with with post hoc Tukey test as appropriate, $P < 0.05$ were considered statistically significant. IC_{50} values were generated using Graphpad Prism's curve fitting feature.

2. Results and Discussion

2.1. Characterization of peptide nanomaterials

Two peptide amphiphiles, containing all *D*-amino acids, BP-k-f-f-v-l-k-$(r)_8$ (CPTNP-FF, fibril competent) and BP-k-G-G-v-l-k-$(r)_8$ (CPTNP-GG, fibril incompetent negative control)

were synthesized on Rink-amide resin via standard Fmoc-based peptide chemistry (Figure 2, A, B). *D*-amino acids were used to increase proteolytic stability in the lysosome and blood plasma. This strategy is effective as the majority of proteolytic enzymes are selective for peptide bonds formed by L-amino acids.[32] Synthesized peptides were cleaved from resins with 95% TFA, 2.5% H_2O, and 2.5% triisopropylsilane for 16 hours. The identity of the peptide product was verified by MALDI-TOF (Figure S1) and ^1H NMR (Figure S2). To observe peptide amphiphile self-assembly, we first dissolved peptide in DMSO at a concentration of 20 mM. To form nanoparticles, DMSO-peptide solution was pipetted into ultra-pure water, phosphate buffered saline or other aqueous solution and quickly vortexed for 30 seconds at the appropriate concentration. To form nanofibrils, an acidic buffer was added to pre-formed nanoparticles in aqueous solution. Nanoparticles remain stable at as low as pH 5.5. Using the above method, we formed peptide nanoparticles and nanofibrils at a 40 μM concentration and measured the particle size via dynamic light scattering (Figure 2, C). Importantly, bis-pyrene is an aggregation induced emission enhanced (AIEE) dye. Because of the AIEE effect, fluorescence of CPTNP monomer in DMSO is notably blue-shifted when compared to the nanomaterial formulation as shown in Figure 2, D.

To demonstrate the pH mediated nanoparticle-nanofiber transformation, DLS measurements were taken at pH 7.4 and pH 4.0. At pH 7.4, the size of CPTNPs was determined to be 15.35 nm at 27 °C, with a poly-dispersity index of 0.194. When the pH was adjusted to 4.0, a secondary peak was detected at 170 nm and a tertiary peak in the μm range, a characteristic DLS signal shift which indicates nanofibril formation as seen previously in Yang et al.[33] It can be noted here that while the fibril competent particles show a substantial shift in the DLS signal indicative of fibril formation, none was seen with the fibril incompetent CPTNP-GG negative control nanoparticle, confirming that FF domain is critical for fibril formation.

The surface charge of CPTNPs was measured using a Malvern Zetasizer. While fibril incompetent CPTNP-GGs exhibited a zeta potential of 13 mV at both pH 7.4 and 4.0. CPTNP-FFs demonstrated a zeta potential of ~13mV at pH 7.4 but the zeta potential was modulated to 26 mV when exposed to a pH of 4.0. This may be due to a shift in exposed arginine groups on the nanomaterial surface. (Figure 2, D)

The critical micelle concentration (CMC) of CPTNP-FFs was calculated to be 0.63μM using the Nile red method.[34] Nile red fluorescence is increased nearly 20 fold in the presence of the hydrophobic core of micellular nanomaterials and may thereby be used to determine the concentration at which nanomaterials are formed. Here, we observed the fluorescence of Nile red (Ex/Em: 485/636nm) on a Spectra Max, M3 plate reader in serially diluted concentrations of CPTNP-FF. We then curve fit the data using Prism's sigmoidal curve fitting function (R^2 =0.9928), and utilized the second derivative method to determine the CMC (Figure 2, E).

Transmission electron microscopy validated that nanofiber were formed when the acidity of the aqueous solution was increased to pH 4.0. The *D*-Phe-*D*-Phe dipeptide motif appeared to be critical for nanofibril formation, as when substituted with a Gly-Gly motif, nanofibrils were not observed, as expected (Figure 2, F).

2.2 Cellular localization of CPTNPs and mechanism of uptake

To determine the intracellular localization of CPTNPs, A549 cells were incubated with both CPTNP and LysoTracker Red DND-99, a dye which, when protonated by an acidic environment, becomes membrane impermeable and is thereby trapped in the acidic lysosome. It was found that CPTNP-FF and CPTNP-GG colocalized with LysoTracker Red DND-99 as seen in Figure 3, A. An intensity heat map of CPTNP and LysoTracker Red was generated using ImageJ and the Pearson's colocalization coefficient was found to be 0.94 in each case (Figure 3, B). To validate that CPTNP-FF was up-taken by the cell, a Z-stack of a single A549 cell was performed. Indeed, BP fluorescence was observed inside the cell, co-localized with LysoTracker Red signal (Figure 3, C). A 3D render of this study is shown in the supplementary material (Figure S3).

Through the course of these uptake studies, an interesting effect was observed whereby after approximately 3 hours of treatment with high concentration CPTNP-FF, the LysoTracker Red signal would rapidly dissipate. To investigate this further, a time-lapse study was conducted using a confocal Zeiss LSM-800 microscope equipped with incubator system to keep a constant temperature of 37°C, by first treating A549 cells with 75 nM LysoTracker Red DND-99 for 30 mins, and subsequent treatment with 50 μM CPTNP for 1 hr. Cells were then washed and imaged every minute beginning at 2.5 hrs. Enough time to allow for the endocytosis of CPTNP-FFs and the initial formation of nanofibers. Here, several punctate LysoTracker Red DND-99 signals were observed to rapidly disperse over time (Figure S4). A single lysosome (red) can be observed to first co-locate with CPTNP (green) then disperse over the course of 30 minutes (Figure 3, D). This is indicative of lysosomal disruption and led us to further study LMP as discussed in Figure 4.

To observe the effect of CPTNPs on cell viability, CPTNP-FF and CPTNP-GGs, at various concentrations were incubated with the cells for 72 hours. After incubation, proliferation was measured via MTS assay, and absorbance was measured at 490 nm via plate reader. While no cytotoxicity was observed for CPTNP-GGs, CPTNP-FF was found to be cytotoxic with an IC_{50} of 2.49 μM (Figure 3, E), indicating that nanofibril formation is required for cytotoxicity. To determine the cytotoxicity of CPTNPs against various cancer cell lines, MTS assays were performed on A549 lung carcinoma cells, A427, H460 non-small cell lung cancer lines, and HPAepic (human primary alveolar cells). The IC_{50} of CPTNP-FF was found to be significantly lower in A549, A427, and H460 cancer cells than the primary HPAepic cells Figure S5.

To determine the mechanism of CPTNP uptake, A549 cells were incubated with CPTNPs and separately with three different endocytic inhibitors: amiloride, an inhibitor of micropinocytosis; β-cyclodextrin, an inhibitor of caveolae-mediated endocytosis; and hypertonic sucrose, an inhibitor of clathrin-mediated endocytosis (CME). Hypertonic sucrose was found to inhibit the cytotoxic effect of CPTNPs, indicating that CME might be required for CPTNP activity (Figure 3, F). Indeed, Figure 3G suggests that clathrin is upregulated in A549 cells when compared to primary HPAepic cells. The importance of CME reinforced by Figure 3, H, which demonstrates that while amiloride and β-cyclodextrin did not inhibit uptake of CPTNP-FF, hypertonic sucrose, a CME inhibitor greatly reduces CPTNP in A549 cells. It has previously been reported that clathrin expression is upregulated

in NSCLC. To validate this, we performed a western blot utilizing A549 NSCLC cells and primary HPAepic cells and stained for clatherin expression. We indeed observed that clathrin was over-expressed in A549 cells. This may explain the discrepancy in CPTNP uptake and IC_{50} values between the two cell lineages documented in Figures S5 and S6. Figure S6 demonstrates that while CPTNP uptake was readily observed in A549 lung carcinoma cells, much less uptake was measured in primary human pulmonary alveolar epithelial cells (HPAepic). The IC_{50} value of HPAepic cells was found to be much higher than A549 cells (25.23μM vs 2.49μM), which is further indicative of the role of CME in CPTNP-FF cytotoxicity. Other factors may play a role in the unequal cytotoxicity, however. Lysosomal associated membrane protein 2 (LAMP2), was also found to be downregulated in A549 cells vs HPAepic cells (Figure S7). Downregulation of LAMP2 has previously been associated with susceptibility to LMP.[2]

2.3 CPTNPS induce lysosomal disruption *in vitro* and *in vivo*

The rapid dissipation of lysotracker signal as seen in Figure 3, D suggests that CPTNPs were inducing lysosomal membrane permeation. To probe the nature of lysosomal disruption, A549 cells were incubated with 200 μg/mL FITC-Dextran (10 kD) for 12 h and subsequently washed and incubated in untreated media for 2 h. Next, these pretreated cells were incubated with varying concentrations of CPTNP-FF for 4 h. In untreated cells, we expected FITC-Dextran to be endocytosed and sequestered in the lysosome, giving a punctate signal. Should the lysosomal membrane be permeated, FITC signal would escape the lysosome and be cytosolically distributed. Because FITC is self-quenched at high local concentrations and quenched in acidic environments, an increase in FITC signal may be used to quantify lysosomal leakage, as depicted in Figure 4, A.[30] This is reflected in our data which shows CPTNP dose dependent FITC signal, an indication of LMP (Figure 4, B). While the FITC-Dextran assay demonstrates that CPTNP-FF induces LMP, the assay sensitivity is limited. To probe the LMP effect of CPTNP-FFs at lower concentrations (1μM in this case) more sensitive galectin puncta assay, previously reported in the literature, was utilized.[31] Briefly, in untreated cells, galectin-1 is cytosolically distributed. However, when the lysosomal membrane is permeabilized, galectin-1 binds to the glycosylated termini of lysosomal membrane associated protein-1 (LAMP-1), and upon fixation and antibody staining for galectin1, reveals a punctate pattern as compared to the uniform cytosolic distribution of galectin-1 in cells with intact lysosomes (Figure 4, C). Figure 4, D shows punctate galectin-1 in A549 cells treated with 1 μM CPTNP-FF for 24 hours but not CPTNP-GG (fibril incompetent nanoparticle) or control. Puncta were tabulated by enumerating the number of puncta and number of cells per image with a minimum of 40 cells per image. Five images were taken per well and averaged. Three wells were averaged to arrive at the final value, demonstrating more puncta/cell in the CPTNP-FF case.

This indicates that CPTNP-FFs induced LMP in a fibril dependent manner, at low dosages (1μM) (Figure 4, D). To determine the LMP activity of CPTNP-FF *in vivo*, athymic mice bearing A549 flank tumors were treated with either 5 mg/kg CPTNP-FF or PBS. Mice were sacrificed 24 hours later, and tumors were harvested, embedded in paraffin, sectioned, and stained for galectin-1 (Figure 4, E). Immunohistochemistry (IHC) revealed a punctate

pattern in the treated tumor, but a uniform distribution pattern in the PBS control, indicating LMP was induced *in vivo*.

To further observe fibril formation *in situ*, transmission electron microscopy was performed. TEM was carried out by treating A549 cells with 10 μM CPTNP for 24 hours, followed by fixation with Karnovsky's fixative for 1 hour and subsequent fixation with 1% osmium tetroxide and 1.5% potassium ferrocyanide in ddH_2O. Samples were dried in progressive increasing concentrations of ethanol. Resin was allowed to infiltrate the sample for 24 hours and to polymerize. Figure 4, F, displays a control and CPTNP-FF treated lysosome. Nanofibers may be seen inside of A549 cell lysosomes (labeled with red arrows). The membrane of the lysosome was disrupted, as seen in the lower right quadrant of the image. Additional high magnification TEM images of treated and control lysosomes may be seen in Figure S8. A wide field image is shown in Figure 4, G below where many lysosomes with abnormal morphology was seen in the treated case, compared to control.

Previous literature has suggested that nanoparticle platforms induce the formation of reactive oxygen species (ROS) in a size-dependent manner, leading to lysosomal dysfunction.[35] A dihydrofluorescein diacetate assay was used to detect induction of ROS formation by CPTNPs (Figure S9). Briefly, cells were preloaded with a non-florescent FITC precursor which, when in contact with ROS species, is modified into the fluorescent FITC. Then cells were treated and placed in a plate reader for continuous monitoring over 12 hours. No increase in fluorescence was observed after treatment with CPTNP-FF, indicating that CPTNP-FFs did not induce LMP by introducing ROS species in the lysosome. Therefore, we suggest CPTNPs did induce LMP via an orthogonal mechanism to previously reported nanomaterials.

Due to the LMP action of CPTNP-FFs, we suspected that CPTNPs might induce non-apoptotic cell death mechanisms. To validate this hypothesis, we performed an annexin V/PI assay, using a desktop flow cytometer. The results indicate an increase in PI+ cells when treated with CPTNPFF but not Annexin V+ cells (Figure S10) This suggests that CPTNPs kill cells by inducing necrotic cell death.

2.4 CPTNPs sensitize A549 cells to cisplatin *in vitro*

To demonstrate the synergistic cytotoxic effect of CPTNPs with cisplatin *in vitro*, we performed a series of MTS assays with varying levels of cisplatin and peptide, and then developed a standard isobologram.[36] We found that while cisplatin alone had an IC_{50} >2μM, 100nM of CPTNP could lower the IC_{50} approximately 4-fold (Figure 5, A). At 100nM CPTNP, the combination index was determined to be 0.259 (Figure 5, A). This indicates that CPTNPs are highly synergistic with cisplatin in A549 cells. To further demonstrate this effect, A549 cells were sequentially treated first with Texas Red-cisplatin (TR-cisplatin) conjugates for 24 hours at 2 μM, then CPTNPs at 10 μM for 4 hours. Cells were then stained with LysoTracker Green (a dye similar to LysoTracker Red), fixed and observed at 63X on a Zeiss LSM 800 confocal microscope. While a punctate pattern was observed in the Texas Red signal of untreated cells, which colocalize with LysoTracker Green, CPTNP treated cells demonstrated a diffuse Texas Red signal (Figure 5, B), further demonstrated by the decrease in Pearsons R coefficient (Figure 5, C). This

indicates that CPTNPs facilitate cytoplasmic distribution of cisplatin. As cisplatin is then freed from the lysosome and cytotoxicity is increased, one would expect an increase in cisplatin DNA adducts, the primary means by which cisplatin induces cell death. Direct evidence of this may be seen in Figure 5, D where A549 cells were treated with cisplatin and CPTNP-FF, then fixed and stained with anti-cisplatin DNA adducts antibody (Sigma-Aldrich: MABE416). Anti-cisplatin DNA adduct signal was clearly enhanced in the cells treated with both CPTNP-FF and cisplatin. Quantification of the increase in anti-cisplatin DNA adducts in the nucleus of A549 cells is shown in Figure 5, D. This result suggests that the LMP activity demonstrated previously is responsible for cisplatin-lysosome escape and therefore CPTNP-cisplatin synergism. A schematic of this mechanism is summarized in Figure 5, E.

2.5 *In vivo* tumor response and localization

To determine the *in vivo* anti-tumor effect and to measure any toxicity of CPTNPs and duel CPTNP-cisplatin therapy, 32 athymic mice were injected subcutaneously with 12×10^6 A549 NSCLC cells in each flank (two tumors per mouse). When tumor burden reached 100 mm^3 the mice were separated into 5 groups: CPTNP-FF (2mg/kg), CPTNP-FF (2mg/kg) + cisplatin (1mg/kg), CPTNP-GG (2mg/kg), CPTNP-GG (2mg/kg) + cisplatin (1mg/kg), and PBS control. Eight doses of each treatment (CPTNP: IV, cisplatin: IP, Figure 6, A) were administered every third day for 21 days as depicted in Figure 6, B. Mice were monitored bi-weekly until the humane endpoint was reached (tumor volume >2000mm^3), tumor volume was monitored via digital caliper (Figure 6, C). Notably, mice treated with CPTNP-FF + cisplatin experienced significantly reduced tumor burden as compared to all other groups, indicating the synergistic action of the CPTNP-FF/cisplatin treatment. After 30 days the tumor volume as measured using digital caliper and the volumes were analyzed via ANOVA with post hoc Tukey test. The following adjusted P values were found, FF-Cisplatin $P = 0.0003$, FF-Cisplatin vs GG-cisplatin, $P= 0.0076$, FF-Cisplatin vs GG, $P < 0.0001$, FF-Cisplatin vs PBS, $P = 0.0014$. All other P values were not significant. This trend was reflected further in the mean survival rate of mice treated with CPTNP-FF + cisplatin, which was nearly two-fold greater than any other group (Figure 6, D, E). Here, the average survival of each group was similarly analyzed (n=6). The P values were as follows: FF-Cisplatin vs FF, GG, and PBS, $P < 0.0001$, FF-cisplatin vs GG-cisplatin, $P = 0.0008$ all other comparisons were not significant. Body weight was monitored on an electronic scale. While some reduction in weight may be observed in CPTNP-FF + cisplatin vs other groups, mice quickly recovered after the treatment was completed. Once the humane endpoint was reached, blood was collected from three of six animals and biochemistry panel was run on a Heska, DRI-CHEM 4000 (Figure 6, F). No significant differences were observed between the CPTNP and PBS treated groups, indicating limited toxicity. While some liver accumulation may be seen in biodistribution data, no changes in total bilirubin, alkaline phosphatase nor ALT were seen indicating limited toxicity. This conclusion is substantiated by murine bodyweight measurements which trend down during cisplatin treatment (but not CPTNP alone) but recover quickly after treatment (Figure 6, G)

To study CPTNP-FF biodistribution and uptake of CPTNPs *in vivo* we injected one mouse with 5 mg/kg nanomaterial and a second mouse with equal volume PBS. Indeed, bis-pyrene

fluorescence was observed to be higher in the tumor site than other tissues (Figure 6, H, I). This is consistent with earlier results, indicating A549 cell preferential uptake. Enhanced permeability and retention, which suggests nanomaterials preferentially locate to the tumor site due to leaky tumor vasculature, may also be an important factor. While some uptake of CPTNP was observed in the liver, no morphological changes were seen in the H&E stain of the liver tissue (Figure S11).

3. Conclusion

In the above study we developed cell penetrating transformable peptide nanomaterials (CPTNPs). We show that these CPTNPs are endocytosed via clathrin mediated endocytosis, where they then localize in the lysosome. Once in the lysosome, these materials are triggered by the lysosomal acidic pH, and transform into high aspect ratio nanofibrils. These nanomaterials then rupture the lysosomal membrane in a fibril-dependent manner. The induced lysosomal membrane permeabilization can then cause the necrosis of non-small cell lung cancer cells at low micromolar concentrations. Importantly, the LMP effect can also free cisplatin sequestered by the lysosome, thereby synergistically increasing the cytotoxic activity of cisplatin in NSCLC. In a xenograft model the combined effect of CPTNPs + cisplatin was shown to be highly efficacious on tumor burden, increasing survival nearly two-fold with almost no effect on toxicity. Cisplatin is an important chemotherapeutic agent for lung cancer, head and neck cancers, bladder cancer, ovarian cancer and testicular cancer. The main dose limiting toxicity of cisplatin is nephrotoxicity. Any relatively non-toxic agent that can synergize cisplatin activity will have great clinical impact on cancer therapy. CPTNPs are the first example of molecular self-assembly used as a lysosomal permeating agent and cisplatin sensitizer. In the future, modifications to this nanoplatform can be developed which improve biodistribution and tumor targeting via the incorporation of stealth peptides and targeting ligands. Such modification will minimize uptake by liver and other organs, and increase tumor uptake, thereby increasing the potency of CPTNPs. In addition, platinum conjugated CPTNPs can be developed for co-delivery of cisplatin with enhanced synergistic effect, such that lower dose of CPTNP will be needed. We believe CPTNP will evolve into an effective intra-cellular molecular self-assembly therapeutic nanoplatform that will have an impact on the future treatment of NSCLC.

Supplementary Material

Refer to Web version on PubMed Central for supplementary material.

Acknowledgements

CB conceived the original concept with help from LW. CB fabricated samples with the help of LZ. CB developed the experimental plan with guidance from LZ, LW, and KL. AD helped with the chemical characterization of the peptides, while YW and WX helped with *in vivo* experiments. The manuscript was written primarily by CB, all authors contributed significant feedback and additions. All authors have given approval to the final version of the manuscript.

Funding Sources

2R01CA115483 (PI: Lam)

1U01CA198880 (PI: Lam)

1R33CA196445 (PI: Lam)

Received: ((will be filled in by the editorial staff))

Revised: ((will be filled in by the editorial staff))

Published online: ((will be filled in by the editorial staff))

Data Availability Statement

The raw data required to reproduce these findings are available to download from https://data.mendeley.com/datasets/pbvr5hgwmt/draft?a=c3173a0b-d4c0-4adb-b138-81fb2d6cc070. Some raw imaging data may be withheld due to technical limitations.

References

[1]. Piao S, Amaravadi RK, Targeting the lysosome in cancer, Ann. N. Y. Acad. Sci. 1371 (2016) 45–54. 10.1111/nyas.12953. [PubMed: 26599426]

[2]. Kallunki T, Olsen OD, Jäättelä M, Cancer-associated lysosomal changes: friends or foes?, Oncogene. 32 (2013) 1995–2004. 10.1038/onc.2012.292. [PubMed: 22777359]

[3]. Safaei R, Larson BJ, Cheng TC, Gibson MA, Otani S, Naerdemann W, Howell SB, Abnormal lysosomal trafficking and enhanced exosomal export of cisplatin in drug-resistant human ovarian carcinoma cells, Mol. Cancer Ther. 4 (2005) 1595–1604. 10.1158/1535-7163.MCT-05-0102. [PubMed: 16227410]

[4]. Chi C, Zhu H, Han M, Zhuang Y, Wu X, Xu T, Disruption of lysosome function promotes tumor growth and metastasis in Drosophila, J. Biol. Chem. 285 (2010) 21817–21823. 10.1074/jbc.M110.131714. [PubMed: 20418542]

[5]. Nilsson C, Roberg K, Grafström RC, Öllinger K, Intrinsic differences in cisplatin sensitivity of head and neck cancer cell lines: Correlation to lysosomal pH, Head Neck. 32 (2010) 1185–1194. 10.1002/hed.21317. [PubMed: 20029982]

[6]. Dielschneider RF, Henson ES, Gibson SB, Lysosomes as Oxidative Targets for Cancer Therapy, Oxid. Med. Cell. Longev. 2017 (2017) 3749157. 10.1155/2017/3749157.

[7]. Dielschneider RF, Henson ES, Gibson SB, Lysosomes as Oxidative Targets for Cancer Therapy, Oxid. Med. Cell. Longev. 2017 (2017) 3749157. 10.1155/2017/3749157.

[8]. Rowson-Hodel AR, Berg AL, Wald JH, Hatakeyama J, VanderVorst K, Curiel DA, Leon LJ, Sweeney C, Carraway KL, Hexamethylene amiloride engages a novel reactive oxygen species- and lysosome-dependent programmed necrotic mechanism to selectively target breast cancer cells, Cancer Lett. 375 (2016) 62–72. 10.1016/j.canlet.2016.02.042. [PubMed: 26944316]

[9]. Mai TT, Hamaï A, Hienzsch A, Cañeque T, Müller S, Wicinski J, Cabaud O, Leroy C, David A, Acevedo V, Ryo A, Ginestier C, Birnbaum D, Charafe-Jauffret E, Codogno P, Mehrpour M, Rodriguez R, Salinomycin kills cancer stem cells by sequestering iron in lysosomes, Nat. Chem. 9 (2017) 1025–1033. 10.1038/nchem.2778. [PubMed: 28937680]

[10]. LeGendre O, Breslin PA, Foster DA, (−)−Oleocanthal rapidly and selectively induces cancer cell death via lysosomal membrane permeabilization, Mol. Cell. Oncol. 2 (2015) e1006077. 10.1080/23723556.2015.1006077.

[11]. Park D, Lee Y, Biphasic Activity of Chloroquine in Human Colorectal Cancer Cells, Dev. Reprod. 18 (2014) 225–231. 10.12717/devrep.2014.18.4.225. [PubMed: 25949192]

[12]. Circu M, Cardelli J, Barr M, O'Byrne K, Mills G, El-Osta H, Modulating lysosomal function through lysosome membrane permeabilization or autophagy suppression restores sensitivity to cisplatin in refractory non-small-cell lung cancer cells, PLoS ONE. 12 (2017). 10.1371/journal.pone.0184922.

[13]. Raj EN, Lin Y-W, Chen C-H, Liu K-K, Chao J-I, Selective Autophagy Pathway of Nanoparticles and Nanodrugs: Drug Delivery and Pathophysiological Effects, Adv. Ther. 3 (2020) 2000085. 10.1002/adtp.202000085.

[14]. Feng Z, Wang H, Wang S, Zhang Q, Zhang X, Rodal AA, Xu B, Enzymatic Assemblies Disrupt the Membrane and Target Endoplasmic Reticulum for Selective Cancer Cell Death, J. Am. Chem. Soc. 140 (2018) 9566–9573. 10.1021/jacs.8b04641. [PubMed: 29995402]

[15]. Yang P-P, Luo Q, Qi G-B, Gao Y-J, Li B-N, Zhang J-P, Wang L, Wang H, Host Materials Transformable in Tumor Microenvironment for Homing Theranostics, Adv. Mater. 29 (2017) 1605869. 10.1002/adma.201605869.

[16]. Gao Y, Shi J, Yuan D, Xu B, Imaging enzyme-triggered self-assembly of small molecules inside live cells, Nat. Commun. 3 (2012) 1033. 10.1038/ncomms2040. [PubMed: 22929790]

[17]. Yang ZM, Xu KM, Guo ZF, Guo ZH, Xu B, Intracellular Enzymatic Formation of Nanofibers Results in Hydrogelation and Regulated Cell Death, Adv. Mater. 19 (2007) 3152–3156. 10.1002/adma.200701971.

[18]. Jeena MT, Palanikumar L, Go EM, Kim I, Kang MG, Lee S, Park S, Choi H, Kim C, Jin S-M, Bae SC, Rhee HW, Lee E, Kwak SK, Ryu J-H, Mitochondria localization induced self-assembly of peptide amphiphiles for cellular dysfunction, Nat. Commun. 8 (2017) 26. 10.1038/s41467-017-00047-z. [PubMed: 28638095]

[19]. Zhang L, Wu Y, Yin X, Zhu Z, Rojalin T, Xiao W, Zhang D, Huang Y, Li L, Baehr CM, Yu X, Ajena Y, Li Y, Wang L, Lam KS, Tumor Receptor-Mediated In Vivo Modulation of the Morphology, Phototherapeutic Properties, and Pharmacokinetics of Smart Nanomaterials, ACS Nano. 15 (2021) 468–479. 10.1021/acsnano.0c05065. [PubMed: 33332957]

[20]. Luo S, Feng J, Xiao L, Guo L, Deng L, Du Z, Xue Y, Song X, Sun X, Zhang Z, Fu Y, Gong T, Targeting self-assembly peptide for inhibiting breast tumor progression and metastasis, Biomaterials. 249 (2020) 120055. 10.1016/j.biomaterials.2020.120055.

[21]. Zhang L, Jing D, Jiang N, Rojalin T, Baehr CM, Zhang D, Xiao W, Wu Y, Cong Z, Li JJ, Li Y, Wang L, Lam KS, Transformable peptide nanoparticles arrest HER2 signalling and cause cancer cell death in vivo, Nat. Nanotechnol. 15 (2020) 145–153. 10.1038/s41565-019-0626-4. [PubMed: 31988501]

[22]. Wang D, Fan Z, Zhang X, Li H, Sun Y, Cao M, Wei G, Wang J, pH-Responsive Self-Assemblies from the Designed Folic Acid-Modified Peptide Drug for Dual-Targeting Delivery, Langmuir. 37 (2021) 339–347. 10.1021/acs.langmuir.0c02930. [PubMed: 33356306]

[23]. Feng Z, Wang H, Chen X, Xu B, Self-Assembling Ability Determines the Activity of Enzyme-Instructed Self-Assembly for Inhibiting Cancer Cells, J. Am. Chem. Soc. 139 (2017) 15377–15384. 10.1021/jacs.7b07147. [PubMed: 28990765]

[24]. Serrano-Puebla A, Boya P, Lysosomal membrane permeabilization as a cell death mechanism in cancer cells, Biochem. Soc. Trans. 46 (2018) 207–215. 10.1042/BST20170130. [PubMed: 29472365]

[25]. Giraldo AMV, Appelqvist H, Ederth T, Öllinger K, Lysosomotropic agents: impact on lysosomal membrane permeabilization and cell death, Biochem. Soc. Trans. 42 (2014) 1460–1464. 10.1042/BST20140145. [PubMed: 25233432]

[26]. Fuchs SM, Raines RT, Pathway for Polyarginine Entry into Mammalian Cells †, Biochemistry. 43 (2004) 2438–2444. 10.1021/bi035933x. [PubMed: 14992581]

[27]. Gross A, Alborzinia H, Piantavigna S, Martin LL, Wölfl S, Metzler-Nolte N, Vesicular disruption of lysosomal targeting organometallic polyarginine bioconjugates, Metallomics. 7 (2015) 371–384. 10.1039/C4MT00255E. [PubMed: 25608481]

[28]. Nir S, Zanuy D, Zada T, Agazani O, Aleman C, Shalev DE, Reches M, Tailoring the self-assembly of a tripeptide for the formation of antimicrobial surfaces, Nanoscale. 11 (2019) 8752–8759. 10.1039/C8NR10043H. [PubMed: 30778487]

[29]. Yang F, Xiao W, Liu Y, Liu R, Kramer R, Li X, Ajena Y, Baehr CM, Rojalin T, Zhang H, Lam KS, One-bead one-compound combinatorial library derived targeting ligands for detection and treatment of oral squamous cancer, Oncotarget. 10 (2019) 5468–5479. 10.18632/oncotarget.27189. [PubMed: 31534631]

[30]. Aits S, Jäättelä M, Nylandsted J, Chapter 13 - Methods for the quantification of lysosomal membrane permeabilization: A hallmark of lysosomal cell death, in: Platt F, Platt N. (Eds.), Methods Cell Biol., Academic Press, 2015: pp. 261–285. 10.1016/bs.mcb.2014.10.032.

[31]. Aits S, Kricker J, Liu B, Ellegaard A-M, Hämälistö S, Tvingsholm S, Corcelle-Termeau E, Høgh S, Farkas T, Jonassen AH, Gromova I, Mortensen M, Jäättelä M, Sensitive detection of lysosomal membrane permeabilization by lysosomal galectin puncta assay, Autophagy. 11 (2015) 1408–1424. 10.1080/15548627.2015.1063871. [PubMed: 26114578]

[32]. Van Breemen RB, Davis RG, Rates of peptide proteolysis measured using liquid chromatography and continuous-flow fast atom bombardment mass spectrometry, Anal. Chem. 64 (1992) 2233–2237. 10.1021/ac00043a009. [PubMed: 1449212]

[33]. Yang P-P, Luo Q, Qi G-B, Gao Y-J, Li B-N, Zhang J-P, Wang L, Wang H, Host Materials Transformable in Tumor Microenvironment for Homing Theranostics, Adv. Mater. 29 (2017) 1605869. 10.1002/adma.201605869.

[34]. Peterson AM, Tan Z, Kimbrough EM, Heemstra JM, 3,3′-Dioctadecyloxacarbocyanine perchlorate (DiO) as a fluorogenic probe for measurement of critical micelle concentration, Anal. Methods. 7 (2015) 6877–6882. 10.1039/C5AY01444A.

[35]. Sabella S, Carney RP, Brunetti V, Ada Malvindi M, Al-Juffali N, Vecchio G, Janes SM, Bakr OM, Cingolani R, Stellacci F, Paolo Pompa P, A general mechanism for intracellular toxicity of metal-containing nanoparticles, Nanoscale. 6 (2014) 7052–7061. 10.1039/C4NR01234H. [PubMed: 24842463]

[36]. Tallarida RJ, Quantitative Methods for Assessing Drug Synergism, Genes Cancer. 2 (2011) 1003–1008. 10.1177/1947601912440575. [PubMed: 22737266]

[37]. Aranda A, Sequedo L, Tolosa L, Quintas G, Burello E, Castell JV, Gombau L, Dichloro-dihydro-fluorescein diacetate (DCFH-DA) assay: A quantitative method for oxidative stress assessment of nanoparticle-treated cells, Toxicol. In Vitro. 27 (2013) 954–963. 10.1016/j.tiv.2013.01.016.

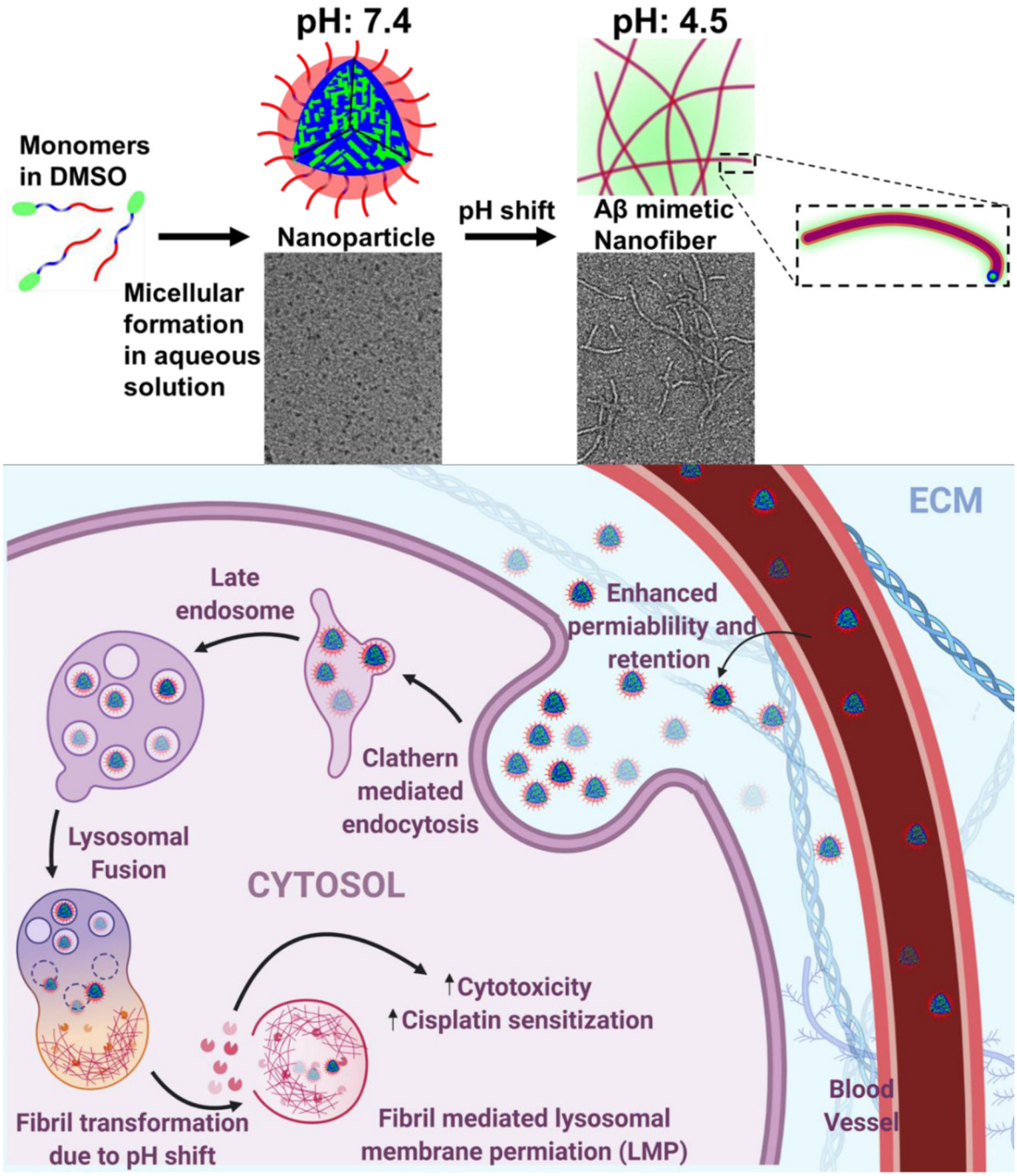

Figure 1.

Schematic of CPTNP action *in vitro* and *in vivo*. Nanomaterials are made by first dissolving peptide amphiphiles in DMSO at 20mM, and then rapidly diluted in pH7.4 aqueous buffer to create nanoparticles. The pH may then be reduced to induce the formation of high aspect ratio nanofibers. Peptide nanoparticles may be incubated with cells or injected IV which circulate and preferentially locate to the tumor sites via the EPR effect. These nanoparticles are taken up by cancer cells and trafficked to the lysosome via CME. The Lysosomal pH shift induces nanofibril formation and lysosomal membrane permeation, thereby releasing

the lysosomal contents into the cytoplasm and inducing LMP mediated cell death and cisplatin sensitization.

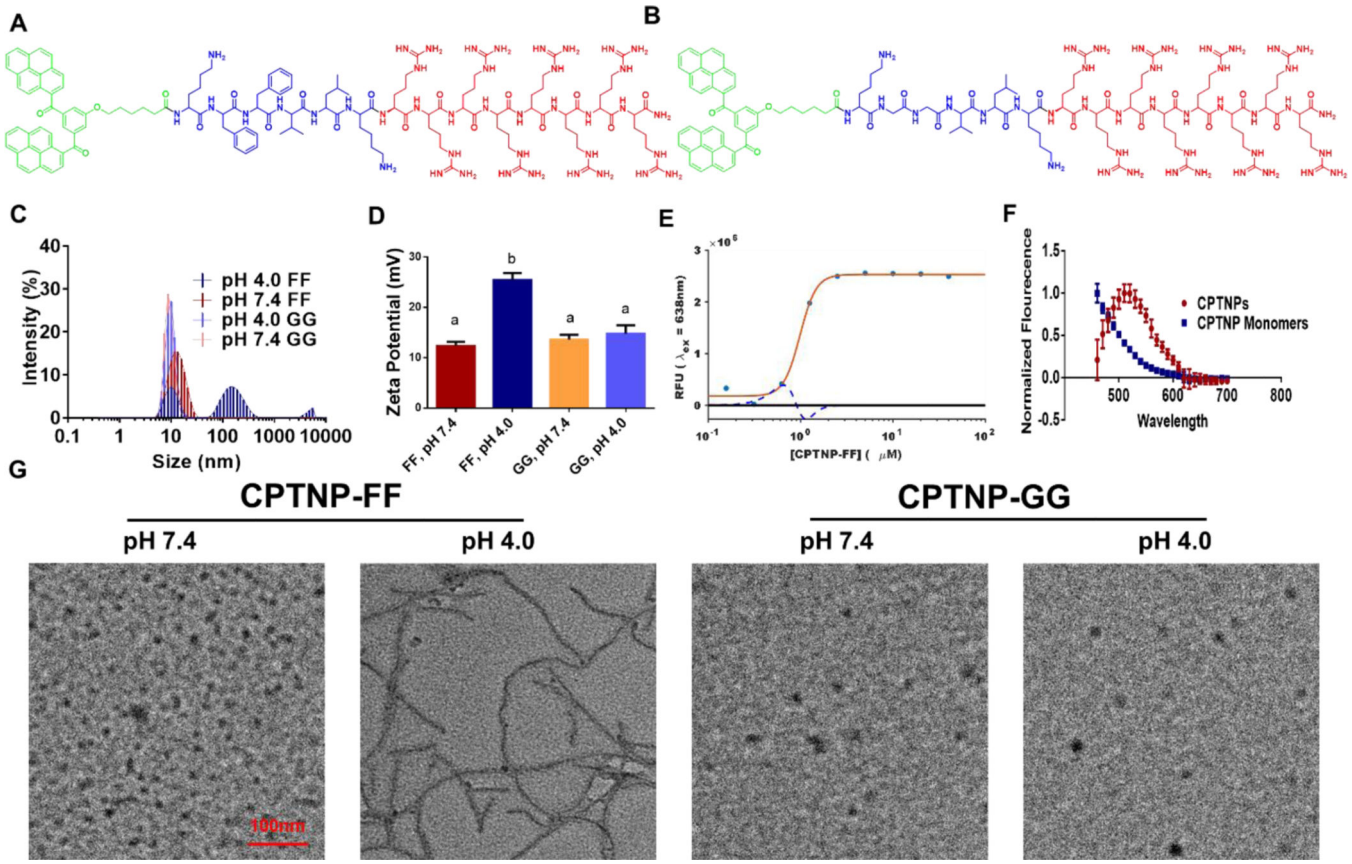

Figure 2.

A. Chemical structure of CPTNPs (BP-k-f-f-v-l-k-$(r)_8$) wherein green depicts bis-pyrene; blue depicts ß-sheet forming motif; red depicts cell-penetrating peptide. **B**. Negative control GG-CPTNP (BP-k-G-G-v-l-k-$(r)_8$) is similar to A except that the Phe-Phe motif was replaced with Gly-Gly motif. **C**. Particle sizes of CPTNPs (FF) and GG-CPTNPs (GG) under various pH, as determined by DLS. **D**. Zeta potential of FF- and GG-CPTNPs measured at 50 μM. (a:b, $p < 0.0005$) **E**. Critical micelle concentration as calculated via nile red fluorescence using the second derivative method. The red line indicates a curve fitted to the fluorescence at 638nm excitation where the blue line is the second derivative of the red curve. CMC = 0.63μM **F**. Fluorescence of CPTNP monomer in DMSO was found to shifted to red when CPTNP nanoparticles was formulated in PBS, due to AIEE effect of BP **G.** TEM images of CPTNPs incubated at pH7.4 and 4.0. Scale bar is 100 nm in each image.

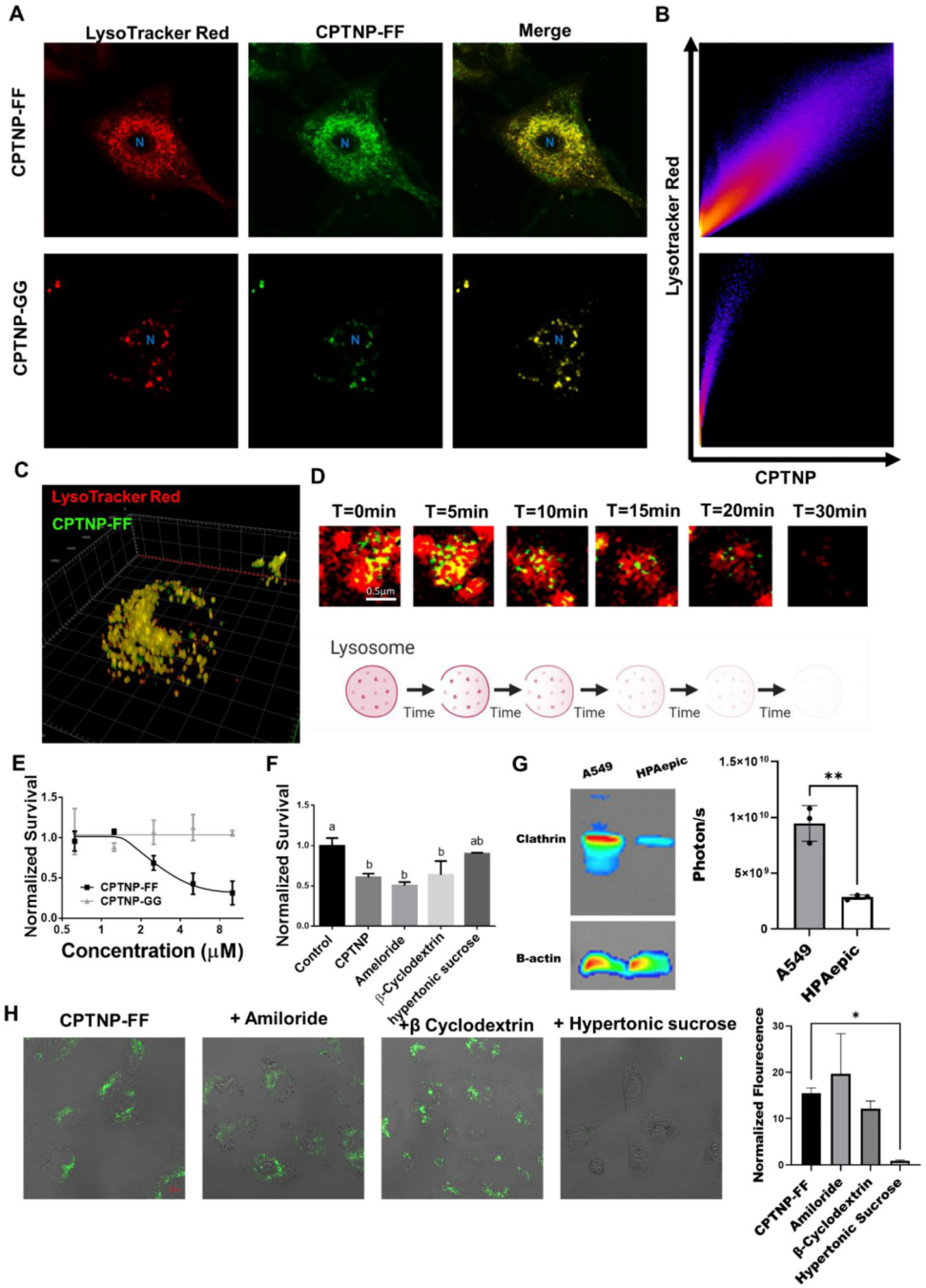

Figure 3.

A. Single A549 cell treated with 1 μM CPTNP-FF and CPTNP-GG stained with 0.75 nM LysoTraker Red DND-99, the nucleolus is represented by a blue N. **B**. Intensity heat map of pixel intensity distribution of a cells imaged after treatment with CPTNP-FF and CPTNP-GG fluorescence and compared via LysoTracker Red fluorescence giving rise to a Pearson's coefficient of 0.94 in each case. **C**. Z stack of a single A549 cell treated with CPTNP-FF (Green) and LysoTraker Red (Red) rendered in 3D indicating true uptake in the interior of the cell. **D.** Live cell confocal image of a single lysosome stained with LysoTraker

Red DND-99 and treated with CPTNP with accompanying illustration. Imaging starts at 2.5 hours after removal of 50 μM CPTNP treatment, the characteristic time point at which lysosomal disfunction was observed. The lysosome can be seen to disperse over the course of 30 minutes. Video of whole cells undergoing this process is shown in the supplementary data. **E**. Normalized cytotoxicity of A549 cells after treatment with CPTNP-FF and CPTNP-GG, indicating fibril formation is needed for cell death. **F**. Cell survival normalized to control (untreated) as measured by MTS assay; all other samples were treated with 5 μM CPTNP-FF for 24 hr when combined with three endocytosis inhibitors. Cytotoxicity is inhibited by hypertonic sucrose, an inhibitor of CME. a>b ($p<0.05$), ab>b except for β-cyclodextrin and is not significantly different than a ($p< 0.05$). **G.** Expression of clathrin in A549 non-small cell lung cancer cells and HPAepic primary cells. The blot was repeated three times and luminescence measured to generate the bar graph to the right. Clathrin can be seen to be over expressed in A549 cells. **H**. Confocal scanning laser microscopy of A549 cells treated with CPTNP-FF and various endocytosis inhibitors. Results were quantified and only hypertonic sucrose was found to be significantly different from CPTNPs alone. These results match the survival data shown in **F** above.

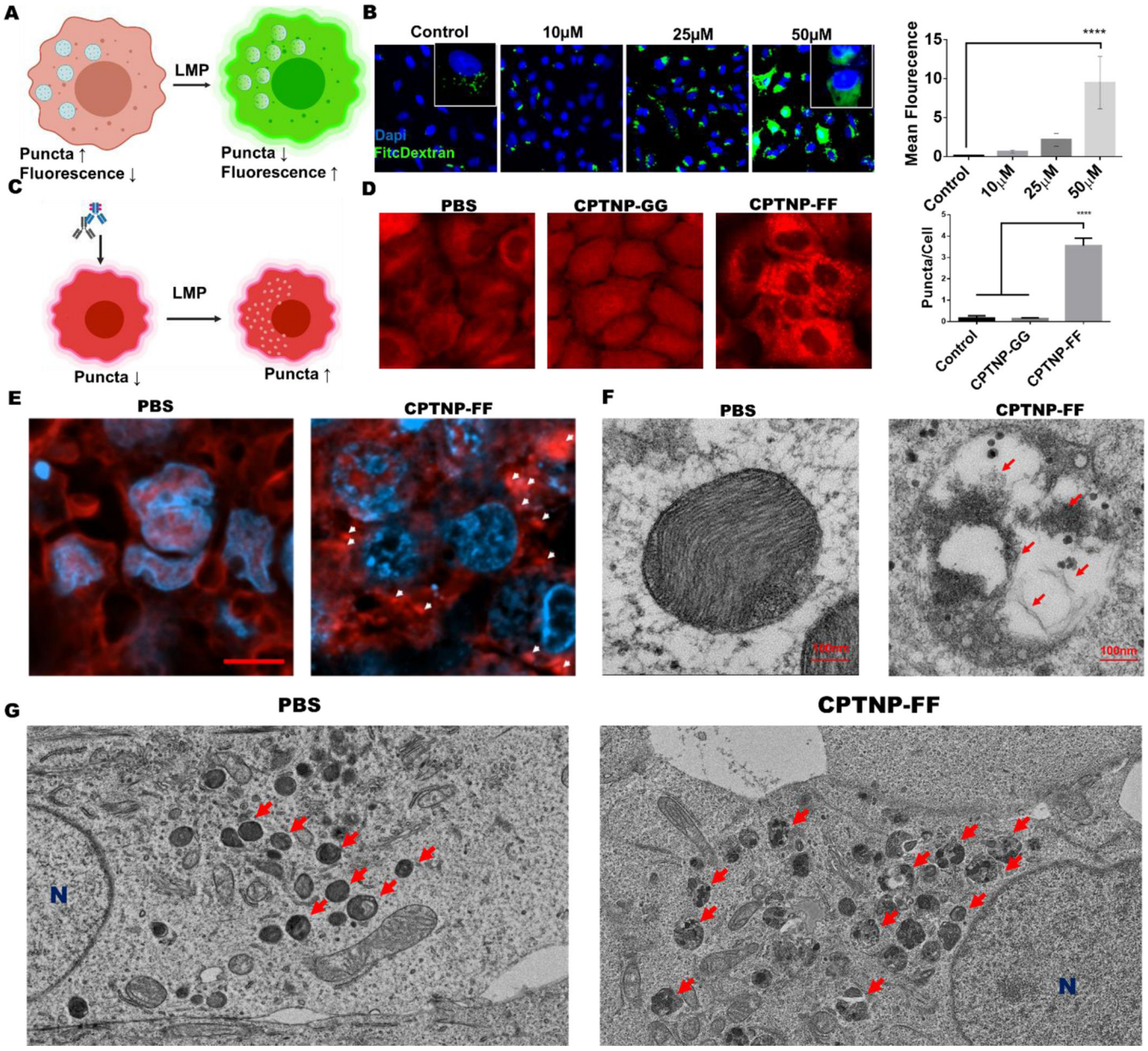

Figure 4.

A. Depiction of expected results from FITC-dextran assay. Briefly when cells are incubated with high concentration 10kDa FITC-dextran, the FITC-dextran is sequestered in the lysosome, where the acidic conditions and high concentration of dye quenches the fluorescence of FITC. When subsequently subjected to lysosomal membrane permeation, the punctate pattern is lost and fluorescence increases. **B.** FITC-dextran assay at varying concentrations, with A549 cells where Green depicts FITC-dextran and blue depicts DAPI. The graph represents the average of 3 wells at various concentrations. The average value of each well was determined by acquiring 5 images and using ImageJ to segment each cell, then measure the average fluorescent intensity. **C.** Illustration of galectin puncta assay where cells may be stained with anti-galectin antibody to reveal either a cytosolic distribution

of galectin-1, indicating no LMP or a punctate distribution of galectin-1, indicating LMP was induced. Galectin-1 has affinity to the glycosylated terminal of lysosome associated membrane protein 1 (LAMP 1) which is only exposed when the lysosome is permeated creating the punctate pattern. **D.** Representative image of a galectin-1 puncta assay with DMSO control and treatment with CPTNP-FF and CPTNP-GG at 1 μM for 24 hr, revealing that lysosomal membrane permeation is fibril dependent. Average puncta/cell was determined by enumerating the number of puncta and number of cells per image with a minimum of 40 cells per image. Five images were taken per well and averaged. Three wells were averaged to arrive at the final value. With accompanying illustration. **E.** Representative images of galectin-1 stained (IHC) tumors 24 hours after treatment with 5 mg/kg CPTNP-FF or PBS. Puncta may be seen in the treated case, highlighted by white arrows Indicating CPTNPs induce LMP *in vivo*. Scale bar is 5 μm. **F.** Transmission electron micrographs of A549 cells after treatment with 10 μM CPTNP for 24 hrs. Nanofibers are labeled with red arrows. Scale bar is 100 nm in each image. **G.** Low magnification TEM image of the same sample, lysosomes are labeled with red arrows while the nucleolus is labeled with a blue N.

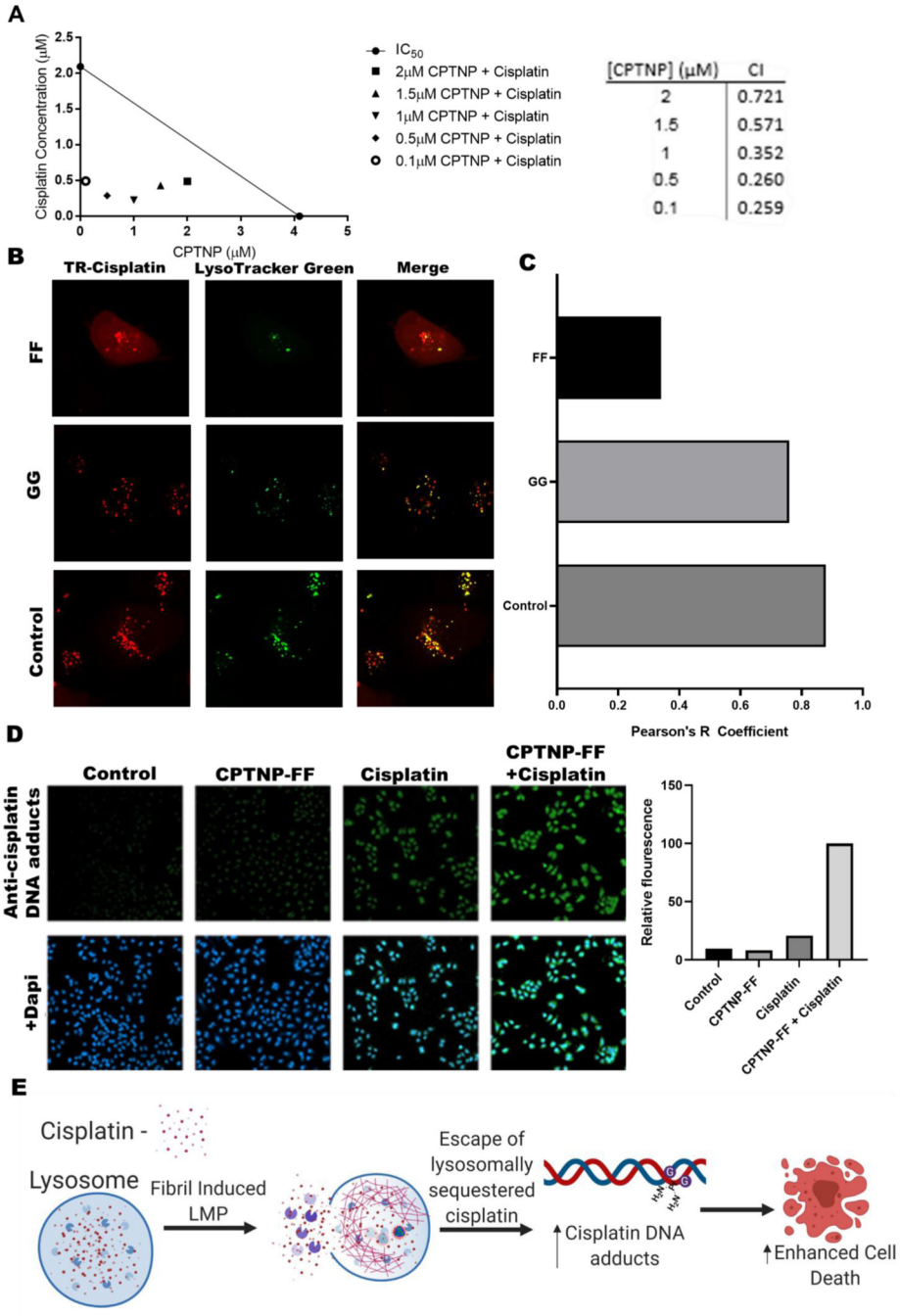

Figure 5.

A. (Left) An isobologram representing the IC_{50} of cisplatin and CPTNPs alone, and combination treatments (48 hr) of cisplatin and CPTNPs in combination with constant CPTNP concentration with varied cisplatin concentration. (Right) the combination index (CI) of each treatment regime using the IC_{50} values documented. **B**. Representative image of TR-Cisplatin treated A549 cells (2 μM) stained with LysoTracker Green with or without CPTNP treatment (10 μM). Where red represents cisplatin, green represents lysotracker green. In the treated case cisplatin can be seen to be cytosolically located. **C**. Pearson's R

coefficient between LysoTracker Green and TR-cisplatin derived from B utilizing ImageJ demonstrating decreased lysosomal sequestration of TR-cisplatin. **D**. To measure the effect of CPTNPs on cisplatin-DNA adducts, cells were treated with cisplatin, CPTNP-FF (2uM) or both and stained with anti-cisplatin DNA adducts. Representative images may be seen, and signal co-located with dapi signal was quantified. Fluorescence intensity was measured and was greatly enhanced in the cisplatin + CPTNP-FF case demonstrating the synergistic effect noted above. **E**. Proposed mechanism of cisplatin sensitization. Cisplatin, sequestered in the lysosome is freed by the LMP action of CPTNPs, allowing for increased availability of cisplatin and increased cell death.

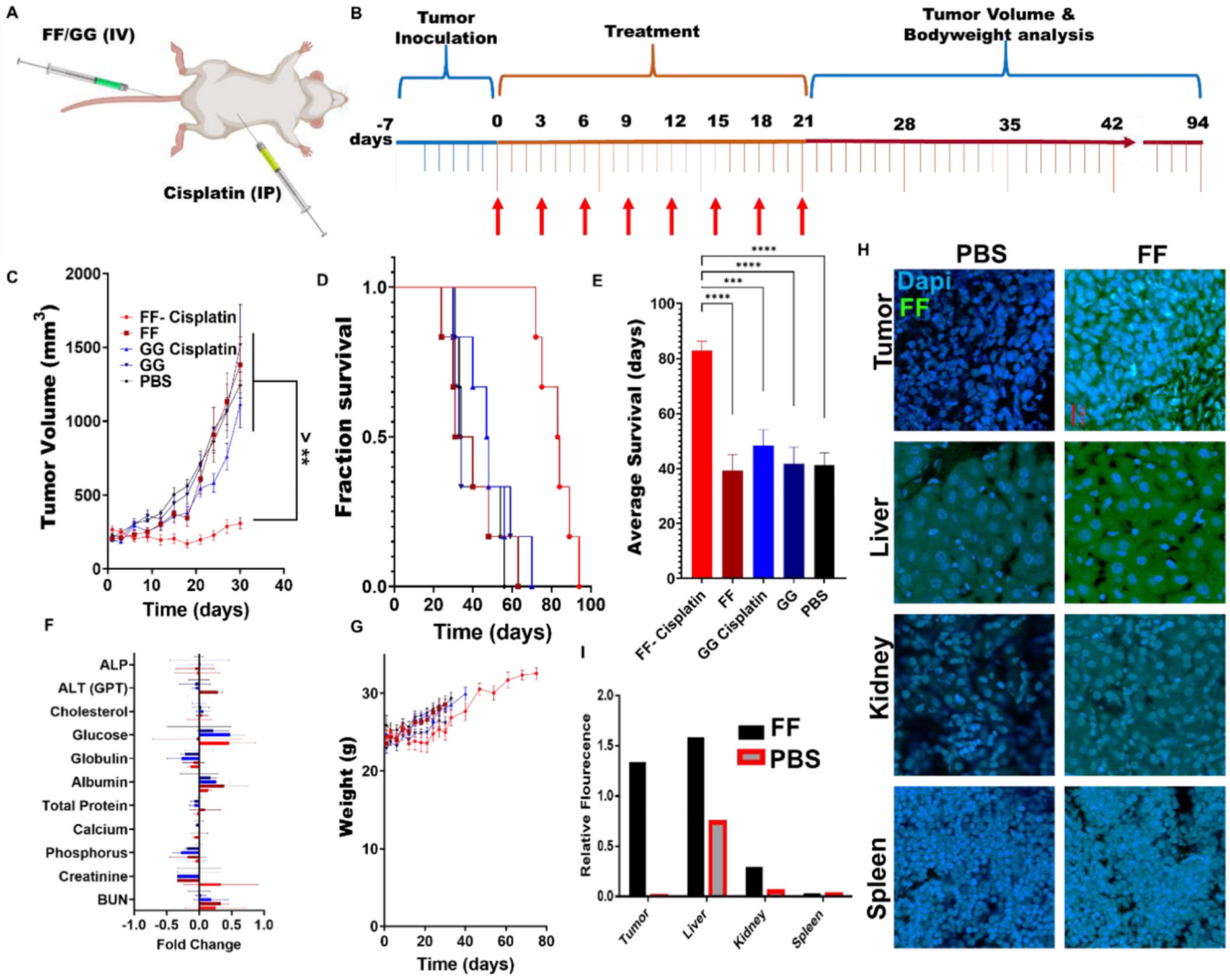

Figure 6.

A. Schema describing IV dosage of CPTNPs (2mg/kg) and IP dosage of cisplatin (1mg/kg) every third day. **B.** schema depicting the study timeline. Mice were inoculated with tumors 7 days before trial start with 12 million cells per tumor, one on each flank (2X/mouse). On day 0 mice were administered one of 5 treatments, CPTNP-FF, CPTNP-FF + cisplatin, CPTNP-GG, CPTNP-GG + cisplatin, PBS(N=6). CPTNPs were dosed at 2mg/kg IV, cisplatin at 1mg/kg IP. Each administered every third day. Tumor volume and bodyweight were measured throughout. Once tumor volume exceeded 2000mm^3 mice were sacrificed. **C**. The documented tumor volume from the above study, once tumor volume exceeded 2000mm^3 mice were sacrificed. Once one third of one trial group reached the humane endpoint, trendlines are no longer reported (Day 30). Tumor volumes were subjected to Anova with post hoc Tukey test. No significant difference was observed between groups FF, GG, GG-cisplatin and PBS. All groups were significantly differentiated from FF-cisplatin ($P < 0.01$), where FF-cisplatin – FF ($P = 0.0003$), FF-cisplatin – GG-cisplatin ($P = 0.0076$), FF-cisplatin – GG ($P < 0.0001$), FF-cisplatin – PBS ($P = 0.0014$). (N= 12) **D.** Kaplan-Meier plot of each group (N=6). **E.** Average survival of each group. (****, P <0.0001; ***,

P<0.001) Statistics were determined via Anova with post hoc Tukey test. **F.** Blood chemistry of mice from the above study (N=3) reported as a fold change from PBS control. No results deviated significantly from the control. Analyzed on a Heska Dri-chem 7000. **G.** Weight of mice from the above study (N=6), reported here until the humane endpoint for 1/3 of mice was reached. **H.** Confocal scanning laser microscopy of *in vivo* tissue samples 24hrs after treatment with 5mg/kg. CPTNP-FF or PBS-Control. Tumor sections can be seen to have high uptake of CPTNP. **I.** Relative fluorescence of comparative samples indicating tumor localization of CPTNPs.